Accurate calibration of geometrical error in reflective surface testing based on reverse Hartmann test

Research Article | Vol. 26, No. 7 | 2 Apr 2018 | OPTICS EXPRESS 8113
Optics EXPRESS

Accurate calibration of geometrical error in reflective surface testing based on reverse Hartmann test

DAODANG WANG,[1,3] ZHIDONG GONG,[1] PING XU,[1] CHAO WANG,[1] RONGGUANG LIANG,[2] MING KONG,[1,4] AND JUN ZHAO,[1]

[1]College of Metrology and Measurement Engineering, China Jiliang University, Hangzhou 310018, China
[2]College of Optical Sciences, University of Arizona, Tucson, Arizona 85721, USA
[3]wangdaodang@sina.com
[4]mkong@cjlu.edu.cn

Abstract: The deflectometry provides a powerful metrological technique enabling the high-precision testing of reflective surfaces with high dynamic range, such as aspheric and freeform surfaces. In the fringe-illumination deflectometry based on reverse-Hartmann-test configuration, the calibration of system geometry is required to achieve "null" testing. However, the system miscalibration can introduce a significant systematic error in the testing results. A general double-step calibration method, which is based on the low-order Zernike aberration optimization and high-order aberration separation, is proposed to separate and eliminate the geometrical error due to system miscalibration. Both the numerical simulation and experiments have been performed to validate the feasibility of the proposed calibration method. The proposed method provides a general way for the accurate calibration of system geometrical error, avoids the over-correction and is feasible for the testing of various complex freeform surfaces.

OCIS codes: (120.6650) Surface measurements, figure; (120.4640) Optical instruments; (120.3940) Metrology.

References and links

1. C. Gannon and R. Liang, "Ray mapping with surface information for freeform illumination design," Opt. Express **25**(8), 9426–9434 (2017).
2. Z. Liu, Y. Pang, C. Pan, and Z. Huang, "Design of a uniform-illumination binocular waveguide display with diffraction gratings and freeform optics," Opt. Express **25**(24), 30720–30731 (2017).
3. A. Bauer, J. P. Rolland, and K. P. Thompson, "Ray-based optical design tool for freeform optics: coma full-field display," Opt. Express **24**(1), 459–472 (2016).
4. T. Yang, G. Jin, and J. Zhu, "Automated design of freeform imaging systems," Light Sci. Appl. **6**(10), e17081 (2017).
5. T. Yang, J. Zhu, and G. Jin, "Compact freeform off-axis three-mirror imaging system based on the integration of primary and tertiary mirrors on one single surface," Chin. Opt. Lett. **14**(6), 060801 (2016).
6. X. Wu, J. Zhu, T. Yang, and G. Jin, "Transverse image translation using an optical freeform single lens," Appl. Opt. **54**(28), E55–E62 (2015).
7. D. Wang, Y. Yang, C. Chen, and Y. Zhuo, "Point diffraction interferometer with adjustable fringe contrast for testing spherical surfaces," Appl. Opt. **50**(16), 2342–2348 (2011).
8. K. Otaki, K. Ota, K. Nishiyama, T. Yamamoto, Y. Fukuda, and S. Okazaki, "Development of the point diffraction interferometer for extreme ultraviolet lithography: Design, fabrication, and evaluation," J. Vac. Sci. Technol. B **20**(6), 2449–2458 (2002).
9. R. Huang, P. Su, T. Horne, G. Brusa, and J. Burge, "Optical metrology of a large deformable aspherical mirror using software configurable optical test system," Opt. Eng. **53**(8), 085106 (2014).
10. P. Su, R. E. Parks, L. Wang, R. P. Angel, and J. H. Burge, "Software configurable optical test system: a computerized reverse Hartmann test," Appl. Opt. **49**(23), 4404–4412 (2010).
11. M. Knauer, J. Kaminski, and G. Hausler, "Phase measuring deflectometry: a new approach to measure specular free-form surfaces," Proc. SPIE **5457**, 366–376 (2004).
12. G. P. Butel, G. A. Smith, and J. H. Burge, "Deflectometry using portable devices," Opt. Eng. **54**(2), 025111 (2015).
13. P. Su, Y. Wang, J. H. Burge, K. Kaznatcheev, and M. Idir, "Non-null full field X-ray mirror metrology using SCOTS: a reflection deflectometry approach," Opt. Express **20**(11), 12393–12406 (2012).

#322522 https://doi.org/10.1364/OE.26.008113
Journal © 2018 Received 6 Feb 2018; revised 13 Mar 2018; accepted 15 Mar 2018; published 20 Mar 2018

Optics EXPRESS

14. D. Wang, S. Zhang, R. Wu, C. Y. Huang, H. N. Cheng, and R. Liang, "Computer-aided high-accuracy testing of reflective surface with reverse Hartmann test," Opt. Express **24**(17), 19671–19681 (2016).
15. C. Andraka, S. Sadlon, B. Myer, K. Trapeznikov, and C. Liebner, "Rapid reflective facet characterization using fringe reflection techniques," J. Sol. Ener. **136**(1), 011002 (2013).
16. M. P. Rimmer, C. M. King, and D. G. Fox, "Computer program for the analysis of interferometric test data," Appl. Opt. **11**(12), 2790–2796 (1972).
17. J. L. Rayces, "Exact relation between wave aberration and ray aberration and ray aberration," J. Mod. Opt. **11**(2), 85–88 (1964).
18. W. H. Southwell, "Wave-front estimation from wave-front slope measurements," J. Opt. Soc. Am. **70**(8), 998–1006 (1980).
19. N. Roddier, "Atmospheric wavefront simulation using Zernike polynomials," Opt. Eng. **29**(10), 1174–1180 (1990).
20. D. Wang, Y. Yang, C. Chen, and Y. Zhuo, "Calibration of geometrical systematic error in high-precision spherical surface measurement," Opt. Commun. **284**(16–17), 3878–3885 (2011).

1. Introduction

With the development of optical design and fabrication, especially the increasing demand of system performance improvement, various types of optical surfaces including aspheric and freeform surfaces have been widely applied in illuminating [1], display [2,3] and imaging systems [4–6], etc. It places ultrahigh requirement on the testing accuracy of the optical elements with complex freeform surfaces, and various methods have been proposed to achieve the accurate testing of optical surfaces. The contact testing with either profiler or coordinate measurement machine (CMM) can achieve high dynamic range, however, the point-to-point scanning process could lead to poor efficiency in the full-aperture measurement. The interferometry provides a powerful testing tool to realize the full-aperture and accurate surface testing, in which the testing accuracy can achieve the order of nanometers [7,8]. However, the dynamic range of interferometric method is quite small, making it not suitable for the freeform surface testing.

The deflectometry can achieve the measurement with high dynamic range [9–11], and it provides a feasible way for the testing of complex freeform surfaces. As a slope measurement method, the deflectometry is a contact-free, high-dynamic-range and full-field testing technique that can measure reflective surfaces with simple and compact system setup. The applications of deflectometry are extremely diverse and it has been applied to test the specular surfaces such as freeform plastic lenses and metal mirrors [12]. A software configurable optical test system (SCOTS), which is based on fringe reflection/deflectometry and reverse Hartmann test, has been successfully implemented in the testing of large astronomy telescope mirrors [10] and precision X-ray mirrors [13] at the University of Arizona. The achievable testing accuracy of deflectometry is mainly determined by calibration process. The calibration error of the geometrical relations among various components in test system, including the tilt, lateral and longitudinal displacements, could introduce evident residual error in the testing result, even though the measurement accuracy of calibration device can reach the order of microns. Besides, the calibration process is quite laborious, complicate and time-consuming. To lower the requirement on the calibration of system geometry, a computer-aided reverse optimization with iterative ray tracing, in which the surface error is taken as the global minimum of the departure from its ideal state, has been proposed to eliminate the additive geometrical errors [14]. However, this optimization method could lead to over-correction and it is more suitable for the precise surface with small error.

In this paper, a general accurate method is proposed for the calibration of geometrical error in the reflective surface testing based on reverse Hartmann test. According to the calibrated test system geometry, the slope data can be obtained from the fringe-illumination deflectometric system, and the virtual "null" surface testing is carried out by ray tracing the modeled test system. The geometric aberrations introduced by various calibration errors of each component in test system are studied in detail, and a general method for system geometry calibration is proposed to remove the geometrical error and achieve accurate surface testing. The proposed general method avoids the over-correction and it is applicable for the testing of freeform

Optics EXPRESS

surface with large aberrations. Section 2 presents the principle of the proposed general method for geometrical error calibration in the reflective surface testing based on reverse Hartmann test, including the system configuration and basic theory of geometrical error calibration. Section 3 shows the simulation results about the test system geometry measurement error and the corresponding calibration method, and experimental results are also given in this section. Finally, some concluding remarks are drawn in Section 4.

2. Principle

2.1. System layout of reverse Hartmann test

The configuration of reverse Hartmann test, that is fringe illumination deflectometry, can be applied to test the reflective surface with high dynamic range, and Fig. 1 shows the system layout for freeform surface testing. In the traditional Hartmann test shown in Fig. 1(a), the point light source placed near the curvature center of test surface sends lights through the Hartmann screen, and a corresponding region of test surface is illuminated. Based on the triangulation, the local surface slopes (w_x, w_y) of the bright point can be determined with the coordinates of the point light source, hole on Hartmann screen and illuminated pixel on detector. The test surface figure can be obtained from the integration of the slopes (w_x, w_y). In the reverse Hartmann test shown in Fig. 1(b), the point light source is replaced by a CCD camera with a finite size of aperture to detect the light reflected from test surface and the detector is replaced by an illumination screen. To obtain the one-to-one correspondence between the illumination screen pixel and the reflection region on test surface, the sinusoidal fringes illumination and phase shifting method can be applied in reverse Hartmann test [15].

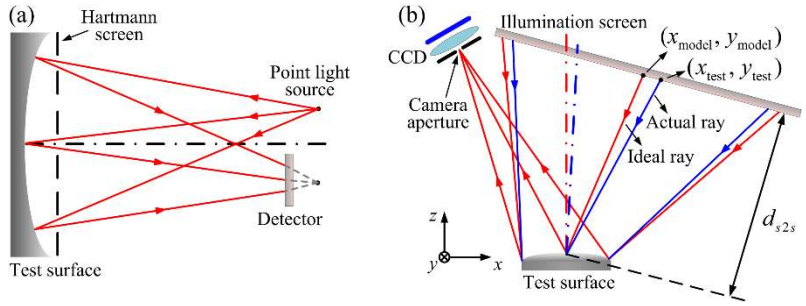

Fig. 1. System layout of the reverse Hartmann test for freeform surface testing. (a) Traditional Hartmann test, (b) reverse Hartmann test for freeform surface testing.

In the reflective surface testing based on reverse Hartmann test, the surface error can be measured according to the virtual "null" testing, in which ray tracing of the test system model obtained from the measured system geometry is performed. The ideal spot distribution (x_{model}, y_{model}) on the image plane can be obtained by ray tracing the test system model with ideal test surface; besides, the actual spot distribution (x_{test}, y_{test}) in the experiment can be measured according to the sinusoidal-fringe phase-shifting method. Based on the transverse ray aberration model [16,17], the wavefront aberration can be obtained from the transverse ray aberration. According to Fig. 1(b), the slope differences $(\Delta w_x, \Delta w_y)$ between the ideal slope and measured slope can be obtained by dividing the spot coordinate differences $(\Delta x_{spot}, \Delta y_{spot})$ with the surface-to-screen distance d_{s2s},

Optics EXPRESS

$$\begin{cases} \Delta w_x = \dfrac{\partial W(x,y)}{\partial x} = \dfrac{x_{\text{test}} - x_{\text{model}}}{2d_{s2s}} = \dfrac{\Delta x_{\text{spot}}}{2d_{s2s}} \\ \Delta w_y = \dfrac{\partial W(x,y)}{\partial y} = \dfrac{y_{\text{test}} - y_{\text{model}}}{2d_{s2s}} = \dfrac{\Delta y_{\text{spot}}}{2d_{s2s}} \end{cases}, \tag{1}$$

where (x, y) are the exit pupil coordinate of test system and $W(x, y)$ refers to the wavefront aberration. According to the surface integration method [18], the surface error map under test can be reconstructed from the slope differences $(\Delta w_x, \Delta w_y)$.

2.2. Analysis of geometric aberration in reverse Hartmann test

According to Fig. 1(b), the system configuration of reverse Hartmann test for complex freeform surface testing is an off-axis setup, in which the illumination screen and camera are displaced laterally from the optical axis of test surface. In the testing of concave surfaces, the aberrations introduced by system geometry measurement error can be well restricted by placing the image plane (and point source) at the curvature center of test surface. However, in the case of convex and freeform surface testing, especially for the testing with short working distance, a significant systematic error could exist due to the miscalibration of test system geometry [14]. The ray tracing of modeled test system can be carried out to study the off-axis aberrations corresponding to various measurement errors of test system geometry (that is the system modeling error). The Zernike polynomials [19], in which the wavefront W can be expressed with a series of orthonormal polynomials $\{Z_i\}$ with coefficients $\{C_i\}$, can be applied to describe the off-axis aberrations, we have

$$W = \sum_{i=1}^{N} (C_i Z_i), \tag{2}$$

where N is the total number of Zernike polynomials. According to the ray tracing results of test system model, the off-axis aberrations introduced by the miscalibration of system geometry can be obtained, mainly including Zernike tilt, defocus, spherical, astigmatism and coma aberrations. Traditionally, the system geometrical error is calibrated simply by setting the corresponding low-order Zernike coefficients (piston, tilt in x and y axes, defocus) to zero [16,20]. However, the residual high-order geometric aberrations could introduce significant systematic error in the testing result, especially in the accurate surface testing.

Without loss of generality, we take the lateral displacement $D_{surf,x}$ of test surface in x axis and tilt $T_{surf,x}$ about x axis as the off-axis aberrations to be analyzed. For the test convex surface with 30 mm aperture diameter and 200 mm curvature radius, in which the working distance d_{s2s}, lateral displacement $D_{surf,x}$ in x axis and tilt $T_{surf,x}$ about x axis are 152 mm, 100 mm and 2 degree, respectively, Fig. 2 shows the aberrations corresponding to various geometrical errors of test convex surface, including the lateral displacement error $\Delta D_{surf,x}$ in x axis and tilt error $\Delta T_{surf,x}$ about x axis. The Zernike terms Z_5 - Z_{11} are the Astigmatism x, Astigmatism y, Coma x, Coma y, Primary Spherical, Trefoil x and Trefoil y aberrations, respectively. According to Fig. 2, obvious high-order aberrations are introduced by the miscalibration of system geometry. The Zernike coefficients of Astigmatism y (Z_6) corresponding to 0.1 mm displacement error $\Delta D_{surf,x}$ in x axis is 0.1035 μm and that of Astigmatism x (Z_5) corresponding to 0.05 degree tilt error $\Delta T_{surf,x}$ about x axis is 0.1370 μm. Thus, a general accurate method for the calibration of system geometrical error is required to achieve the accurate testing of various surfaces (especially the freeform surfaces).

Optics EXPRESS

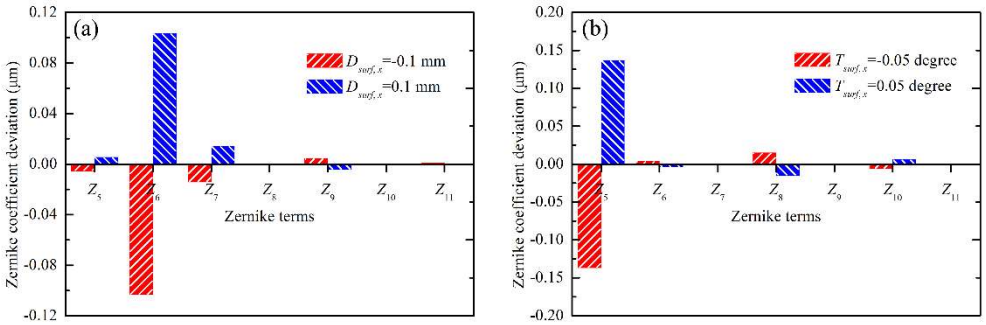

Fig. 2. Zernike coefficient deviations introduced by geometrical error of test convex surface with the 15 mm semi-diameter and 200 mm curvature radius. (a) Lateral displacement error in *x* axis and (b) tilt error about *x* axis.

2.3. Calibration of system geometrical error

In the virtual "null" testing of reflective surfaces based on reverse Hartmann test, the ray tracing of test system model is performed to remove the systematic error due to system geometry. To build the test system model, the geometrical parameter $\mathbf{GP}=\{D_{m,j};T_{m,j}\}_{m=surf,sreen;\,j=x,y,z}$, including the decenter $D_{m,j}$ and tilt $T_{m,j}$ of the m_{th} component in j_{th} direction, are measured with three-dimensional positioning instruments. Due to the accuracy limitation of measuring instruments, the additional measurement error introduced by the miscalibration of system geometry is not negligible, especially in the accurate testing of convex freeform surface with high dynamic range and finite working distance. Denote the systematic geometric aberration introduced by the initial geometrical error $\mathbf{GE}=\{\varepsilon_k\}$ of test system as $W_{geo}^{(0)}$, in which ε_k refers to the k_{th} geometrical error in the geometrical parameter $\mathbf{GP}$, and we have the corresponding measured wavefront aberration $W_{meas}^{(0)}$,

$$W_{meas}^{(0)}=W_{surf}+W_{geo}^{(0)}(\mathbf{GE})=\sum_{i=1}^{N}\left[C_{meas,i}^{(0)}Z_i\right], \tag{3}$$

where W_{surf} is the true surface error under test, $\{C_{meas,i}^{(0)}\}$ are the Zernike coefficients of the measured wavefront aberration $W_{meas}^{(0)}$.

To separate the geometric aberrations from various components in test system, the geometric aberration $W_{geo}^{(0)}$ in Eq. (3) can be expressed as

$$W_{geo}^{(0)}(\mathbf{GE})=\sum_{k=1}^{M}W_{geo}^{(0)}(\varepsilon_k)=\sum_{i=1}^{N}\left\{\left[\sum_{k=1}^{M}C_{geo,i}^{(k)}\right]Z_i\right\}, \tag{4}$$

where *M* is the total number of system geometrical parameters, and $\{C_{geo,i}^{(k)}\}$ are the Zernike coefficients of the geometric aberration $W_{geo}^{(0)}(\varepsilon_k)$ introduced by the k_{th} geometrical error ε_k.

The function $\Gamma_i^{(k)}$ can be applied to describe the relationship between the i_{th} Zernike coefficient $C_{geo,i}^{(k)}$ and the k_{th} geometrical error ε_k. Due to the fact that the measurement of system geometry with three-dimensional positioning instruments provides good initial value and the geometrical error $\mathbf{GE}=\{\varepsilon_k\}$ can be eliminated in a small range, the relationship

between the i_{th} Zernike coefficient $C_{geo,i}^{(k)}$ and the k_{th} geometrical error ε_k can be linearly approximated as

$$C_{geo,i}^{(k)} = \Gamma_i^{(k)}(\varepsilon_k) \cong \rho_i^{(k)}\varepsilon_k, \tag{5}$$

where the slope $\rho_i^{(k)}$ of fitted line refers to the weight of the k_{th} geometrical error ε_k in the i_{th} Zernike coefficient $C_{geo,i}^{(k)}$. To achieve the accurate calibration of geometrical error, a double-step calibration method based on the low-order Zernike aberration optimization and high-order aberration separation can be applied to remove the residual aberrations.

2.3.1. First-step calibration based on low-order Zernike aberration optimization

According to the weights $\{\rho_i^{(k)}\}_{i=1,2,3,4}$ of the geometrical errors $\{\varepsilon_k\}$ in the first four Zernike coefficients $\{C_{geo,i}^{(k)}\}_{i=1,\ldots,4}$ (piston, tilt in x and y axes, defocus), the geometrical error $\mathbf{GE} = \{\varepsilon_k\}$ can be divided into two groups: $\mathbf{GE} = \{\mathbf{GE}^{(H)}, \mathbf{GE}^{(L)}\}$, in which $\mathbf{GE}^{(H)}$ and $\mathbf{GE}^{(L)}$ refer to the geometrical errors with heavy and light weights in first four Zernike terms, respectively. The geometrical error $\mathbf{GE}^{(H)}$ can be pre-calibrated in the first-step calibration according to the objective function $O_1(\mathbf{GE}^{(H)})$,

$$O_1(\mathbf{GE}^{(H)}) = \min\left[\left(\widehat{W}_{geo,4}\right)^2 + c\right], \tag{6}$$

where $\widehat{W}_{geo,4}$ is the geometric aberration corresponding to the first four Zernike terms in the pre-optimization process, and c is an additional constraint to restrict the solution space.

The low-order aberrations are optimized according to the geometrical error $\mathbf{GE}^{(H)}$ in the first-step calibration, the remaining geometrical error $\mathbf{GE}^{(L)}$ with light weights could lead to the existence of residual geometrical error $\mathbf{GE}_1^{(H)}$ with heavy weight and the problem of over-correction. Denoting the residual geometrical error and the corresponding measured wavefront aberration after pre-calibration as $\mathbf{GE}_1 = \{\mathbf{GE}_1^{(H)}, \mathbf{GE}^{(L)}\} = \{\tilde{\varepsilon}_k\}$ and $W_{meas}^{(1)}$, respectively, we have

$$W_{meas}^{(1)} = \sum_{i=1}^{N}\left[C_{meas,i}^{(1)} Z_i\right] \cong \sum_{i=1}^{N}\left\{\left\{C_{meas,i}^{(0)} - \sum_{k=1}^{M}\left[\rho_i^{(k)}(\varepsilon_k - \tilde{\varepsilon}_k)\right]\right\} Z_i\right\}, \tag{7}$$

where $\{C_{meas,i}^{(1)}\}$ are the Zernike coefficients of the measured wavefront aberration $W_{meas}^{(1)}$.

According to Eq. (5), we have the geometric aberration $W_{geo}^{(1)}(\mathrm{GE}_1)$ after first-step calibration,

$$W_{geo}^{(1)}(\mathbf{GE}_1) = \sum_{k=1}^{M} W_{geo}^{(1)}(\tilde{\varepsilon}_k) = \sum_{i=1}^{N}\left\{\left\{\sum_{k=1}^{M}\left[\rho_i^{(k)}\tilde{\varepsilon}_k\right]\right\} Z_i\right\}. \tag{8}$$

After the first-step calibration based on low-order Zernike aberration optimization, the major geometric aberrations, which are mainly introduced by the geometrical errors with heavy weights, can be well eliminated. To avoid over-correction and further calibrate the high-order geometric aberrations in the measured wavefront $W_{meas}^{(1)}$, a second-step calibration based on high-order aberration separation needs to be carried out.

2.3.2. Second-step calibration based on high-order aberration separation

Denote the ratio of the i_{th} Zernike coefficient $C_{geo,i}^{(k)}$ introduced by the k_{th} geometrical error $\tilde{\varepsilon}_k$ to that $C_{geo,i}^{(\tau)}$ corresponding to an arbitrarily component $\tilde{\varepsilon}_\tau$ in the geometrical error $\mathbf{GE}^{(L)}$ with light weight as $r_{k,i}$. According to Eq. (5) and we have

$$r_{k,i} = \frac{C_{geo,i}^{(k)}}{C_{geo,i}^{(\tau)}} \cong \frac{\rho_i^{(k)} \tilde{\varepsilon}_k}{\rho_i^{(\tau)} \tilde{\varepsilon}_\tau}, \tag{9}$$

where $\rho_i^{(\tau)}$ is the weight of the geometrical error component $\tilde{\varepsilon}_\tau$ in the i_{th} Zernike coefficient $C_{geo,i}^{(\tau)}$.

For the initial geometrical error could be estimated from the measurement accuracy of three-dimensional positioning instrument, the Zernike coefficients caused by the residual geometrical error $\mathbf{GE}_1^{(H)}$ can be calculated according to Eq. (9). Assuming the estimated initial geometrical error $\tilde{\varepsilon}_\tau$ is e_τ, we have the geometric aberration $W_{geo}^{(H)}$ corresponding to the residual geometrical error $\mathbf{GE}_1^{(H)}$,

$$W_{geo}^{(H)} = \sum_{i=1}^{N} \left\{ \left[\sum_{k=1}^{s} \left(r_{k,i} \rho_i^{(\tau)} e_\tau \right) \right] Z_i \right\}, \tag{10}$$

where s is the total component number in the geometrical error $\mathbf{GE}_1^{(H)}$. Thus, the remaining geometrical error $\mathbf{GE}^{(L)}$ with light weight can be calibrated according to the objective function $O_2(\mathbf{GE}^{(L)})$,

$$O_2\left(\mathbf{GE}^{(L)}\right) = \min\left[\left(\widehat{W}_{geo}^{(L)} \right)^2 + c \right] = \min\left[(W_{meas}^{(2)} - W_{meas}^{(1)} - W_{geo}^{(H)})^2 + c \right], \tag{11}$$

where $\widehat{W}_{geo}^{(L)}$ is the geometric aberration caused by the geometrical error $\mathbf{GE}^{(L)}$ with light weight, $W_{meas}^{(2)}$ is the measured wavefront aberration in second-step calibration.

According to Eq. (10), the objective function $O_2(\mathbf{GE}^{(L)})$ can be further modified as

$$O_2\left(\mathbf{GE}^{(L)}\right) = \min\left\{ \left\{ \sum_{i=1}^{N} \left[C_{meas,i}^{(2)} - C_{meas,i}^{(1)} - \sum_{k=1}^{s} \left(r_{k,i} \rho_i^{(\tau)} \tilde{\varepsilon}_\tau \right) \right] \right\}^2 + c \right\}_{\tilde{\varepsilon}_\tau \neq 0}, \tag{12}$$

where $\left\{ C_{meas,i}^{(2)} \right\}$ are the Zernike coefficients of the measured wavefront $W_{meas}^{(2)}$ in second-step calibration, and the geometrical error $\tilde{\varepsilon}_\tau$ is a component of the geometrical error $\mathbf{GE}^{(L)}$. With the optimal geometrical parameter $\mathbf{GP}^*$ after calibration of the geometrical error $\mathbf{GE}^{(H)}$ with heavy weight in the first-step calibration and that $\mathbf{GE}^{(L)}$ with light weight in the second-step calibration, respectively, the testing surface error W_{surf} can be obtained as

$$W_{surf} \cong W_{meas}^{(0)} - W_{geo}^{(0)}\left(\mathbf{GE}^{(H)}, \mathbf{GE}^{(L)}\right). \tag{13}$$

Figure 3 shows the whole procedure of reflective surface testing based on reverse Hartmann test, in which the proposed general accurate method is carried out to calibrate the geometrical error. After setting up reverse Hartmann test system, the measured geometrical parameter $\mathbf{GP}$ is applied to build the test system model in ray-tracing software. The wavefront aberration

$W_{meas}^{(0)}$, including the test surface error W_{surf} and geometrical error $W_{geo}^{(0)}$, is measured in test system, in which the virtual "null" test by ray tracing test system model is carried out. According to the proposed double-step calibration method shown in Fig. 3(b), the geometrical error $\mathbf{GE}$ can be calibrated and the optimized geometrical parameter $\mathbf{GP}^*$ is applied to update the test system model, based on which the true test surface error W_{surf} can be obtained. The procedure of double-step calibration is shown in Fig. 3(b). After calculating the weight $\rho_i^{(k)}$ of the k_{th} geometrical error ε_k in the i_{th} Zernike coefficient $C_{geo,i}^{(k)}$, the geometrical error $\mathbf{GE}^{(H)}$ with heavy weight can be optimized in first-step calibration based on low-order Zernike aberration optimization. In the meantime, the iterative ray tracing is performed once after each round of geometrical parameter optimization to update the measured geometric aberration $\hat{W}_{geo,4}$ corresponding to the first four Zernike terms. The optimization repeats until the objective function $O_1(\mathbf{GE}^{(H)})$ reaches a threshold δ_1, then the geometrical error $\mathbf{GE}^{(L)}$ can be set as variable in the second-step calibration based on high-order aberration separation. After calculating the ratio $r_{k,i}$ of the i_{th} Zernike coefficient $C_{geo,i}^{(k)}$ introduced by the k_{th} geometrical error $\tilde{\varepsilon}_k$ to that $C_{geo,i}^{(\tau)}$ corresponding to an arbitrarily component $\tilde{\varepsilon}_\tau$ in the geometrical error $\mathbf{GE}^{(L)}$ with light weight, the optimization of the geometrical error $\mathbf{GE}^{(L)}$ repeats until the objective function $O_2(\mathbf{GE}^{(L)})$ reaches a threshold δ_2, and then the optimized geometrical parameter $\mathbf{GP}^*$ can be obtained.

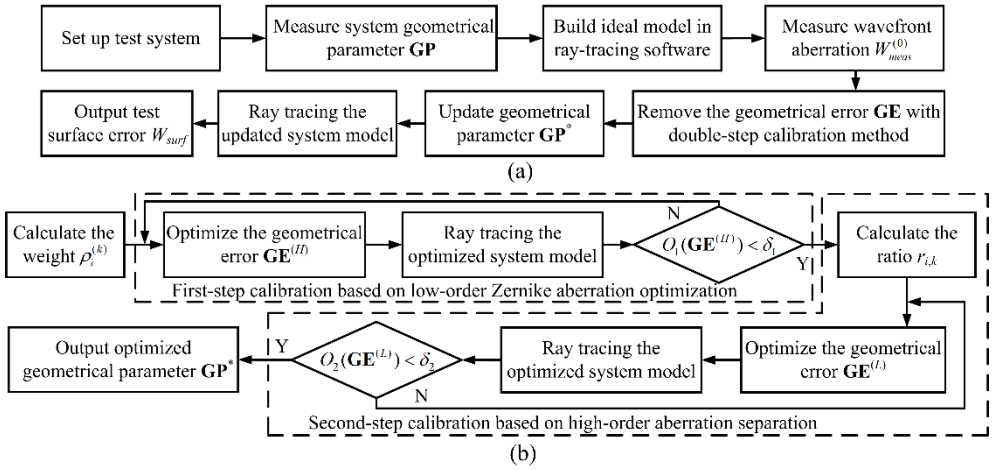

Fig. 3. Procedure for reverse Hartmann test. (a) The whole test procedure, and (b) procedure for double-step calibration of systematic error.

3. Numerical simulation and experimental results

To validate the feasibility and accuracy of the proposed general method for the geometrical error calibration in reflective surface testing based on reverse Hartmann test, both the numerical simulation and experiments have been carried out, in which the wavefront aberration is characterized with 37-term Zernike coefficients.

3.1. Numerical simulation results

In the numerical simulation, a test system based on reverse Hartmann test is modeled in the ray-tracing software (Zemax) according to the configuration shown in Fig. 1(b), in which the test surface is a convex freeform surface with the aperture diameter 30 mm, best fit sphere

Optics EXPRESS

radius 198.2866 mm and best fit sphere vertex offset −5.9809 μm. In the test system, the displacements of test surface in x, y and z axes, tilts of test surface about x and y axes, displacement of illumination screen in z axis, tilts of illumination screen about x and y axes are $D_{surf,x}$ = 100 mm, $D_{surf,y}$ = 0 mm, $D_{surf,z}$ = 150 mm, $T_{surf,x}$ = −2 degree, $T_{surf,y}$ = 2 degree, $D_{screen,z}$ = 152 mm, $T_{screen,x}$ = 1 degree and $T_{screen,y}$ = −1 degree, respectively. Figure 4(a) shows the actual test surface error, whose peak-to-valley (PV) and root-mean-square (RMS) values are 18.4409 μm and 3.1329 μm, respectively.

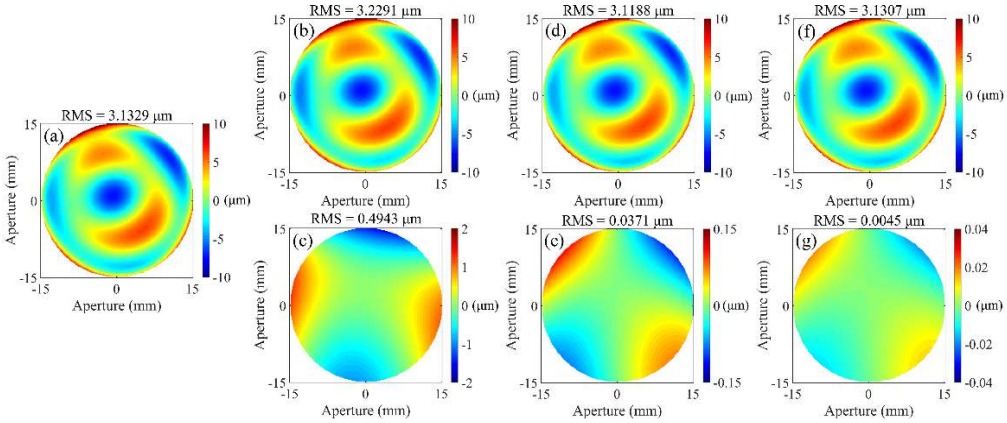

Fig. 4. Surface testing results in the simulation. (a) Actual surface error, (b) testing surface error and (c) residual error with existence of system geometrical error, (d) testing surface error and (e) residual error after first-step calibration, (f) testing surface error and (g) residual error after second-step calibration.

Figures 5(a) and 5(b) show the Zernike coefficient deviations (Z_5-Z_8) corresponding to various displacement errors $\Delta D_{surf,x}$ of test surface in x axis and tilt errors $\Delta T_{surf,x}$ of test surface about x axis, respectively. According to Fig. 5, a good linearity can be seen in the relationship between the Zernike coefficients of geometric aberration and geometrical errors, demonstrating the feasibility of linear approximation in Eq. (5).

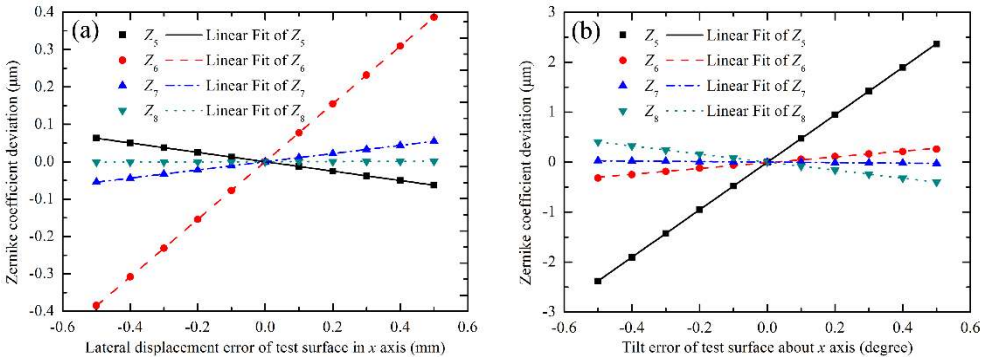

Fig. 5. Linearity about Zernike coefficients of system geometrical error. Zernike coefficient deviations due to (a) lateral displacement error of test surface about x axis and (b) tilt error of test surface about x axis.

To analyze the effect of test system geometrical error on the surface testing result, additional displacement deviations of test surface in x, y and z axes ($\Delta D_{surf,x}$ = $\Delta D_{surf,y}$ = −0.02 mm, $\Delta D_{surf,z}$ = 0.01 mm), tilt errors of test surface about x and y axes ($\Delta T_{surf,x}$ = 0.04 degree, $\Delta T_{surf,y}$ = −0.05 degree), displacement deviations of illumination screen in z axis

Optics EXPRESS

($\Delta D_{screen,z}$ = –0.02 mm), tilt errors of illumination screen about x and y axes ($\Delta T_{screen,x}$ = –0.03 degree, $\Delta T_{screen,y}$ = 0.04 degree), are added to test system geometry in the ray tracing model. Figure 4(b) exhibits the measured surface error with the added system geometrical error and the Gauss noise with RMS value 5 nm, and Fig. 4(c) shows the corresponding residual error with respect to the actual surface error in Fig. 4(a). From Fig. 4(c), a significant error with the PV value 2.7858 μm and RMS 0.4943 μm can be seen in the testing result.

According to Subsection 2.3, the calibration of geometrical error with the proposed double-step calibration method is performed. Figures 4(d) and 4(f) show the measured surface error after the first-step calibration based on low-order Zernike aberration optimization and that after the second-step calibration based on high-order aberration separation, respectively, Figs. 4(e) and 4(g) are the corresponding residual errors with respect to the true test surface error in Fig. 4(a). Figure 6 presents the change about the Zernike coefficients of residual geometric aberration in the calibration process, and Table 1 summarizes the numerical simulation results.

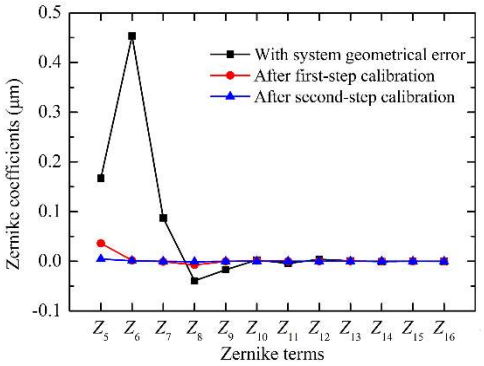

Fig. 6. Change about Zernike coefficients (Z_5-Z_{16}) of residual geometric aberration in calibration process.

Table 1. PV and RMS values of testing surface error in the simulation

	PV (μm)	RMS (μm)
Actual surface error	18.4409	3.1329
With system geometrical error		
Testing surface error	19.4256	3.2291
Residual error	2.7858	0.4943
After first-step calibration		
Testing surface error	18.3861	3.1188
Residual error	0.2138	0.0371
After second-step calibration		
Testing surface error	18.4520	3.1307
Residual error	0.0361	0.0045

Table 2 shows the change about the geometrical error in the calibration process in the simulation. According to Table 2, Figs. 4(e) and 6, the geometrical error is greatly eliminated after first-step calibration. The PV and RMS values of residual geometric aberration after first-step calibration are 0.2138 μm and 0.0371 μm, respectively, and the corresponding Zernike terms mainly include Astigmatism x (Z_5) and Coma y (Z_8). From Figs. 4(g) and 6, the geometrical error can be further removed after second-step calibration, with the PV and RMS values of residual error being 0.0361 μm and 0.0045 μm, respectively. Thus, the proposed double-step calibration method provides a feasible and general way to separate the system geometric aberration from test surface error, addressing the uncertainty on the measurement of system geometry and enabling the accurate testing of various complex surfaces.

Optics EXPRESS

Table 2. Change about the geometrical error in the calibration process

	$\triangle D_{surf,\ x}$ (mm)	$\triangle D_{surf,\ y}$ (mm)	$\triangle D_{surf,\ z}$ (mm)	$\triangle_{Tsurf,\ x}$ (degree)	$\triangle_{Tsurf,\ y}$ (degree)	$\triangle D_{screen,\ z}$ (mm)	$\triangle T_{screen,\ x}$ (degree)	$\triangle T_{screen,\ y}$ (degree)
Geometrical error	–0.02	–0.02	0.01	0.04	–0.05	–0.02	–0.03	0.04
After first-step	–0.002	–0.02	0.002	0.001	–0.001	–0.02	–0.03	0.0009
Second-step calibration	–0.001	–0.001	0.001	0.001	–0.001	–0.003	–0.004	0.0009

3.2. Experimental results

An experimental reverse Hartmann test system according to Fig. 1(b) has been set up to verify the feasibility of the proposed calibration method for the reflective surface testing. The reflective surface to be measured is a diamond-turning convex freeform surface with 100 mm in radius of curvature and 50.8 mm in diameter, whose conic constant is –6.8896. The pixel number of CCD camera is 1328 (H) × 1048 (V), the focal length of imaging lens on camera is 12 mm and the pixel number of LCD projection screen is 1920 (H) × 1080 (V). The system geometry parameter including the positions of camera aperture, test surface and illumination screen, was measured by a CMM (Hexagon Metrology Global Classic, accuracy 5.0 μm and resolution 0.078 μm). The system model was built in the ray-tracing software ZEMAX according to the result of the measured geometrical parameter in CMM. The distance d_{s2s} between test freeform surface and illumination screen is about 180 mm.

Figure 7(a) shows the freeform surface error measured with reverse Hartmann test system based on CMM-measured system geometrical parameter. The proposed double-step calibration method was applied to calibrate the system geometrical error, the measured surface error after first-step calibration and second-step calibration are shown in Figs. 7(b) and 7(c), respectively, with the corresponding changes being shown in Figs. 7(e) and 7(f). Compared with the testing result in Fig. 7(a), the absolute PV differences in Figs. 7(b) and 7(c) are 0.4538 μm and 0.4614 μm, respectively. In order to verify the feasibility of the proposed method for larger geometrical error, an additional deviation (100 μm) of test surface in *x* axis was added in CMM-measured system geometrical parameter, and Fig. 7(d) shows the corresponding testing result after double-steps calibration. Figure 7(g) shows the freeform surface error measured with a ZYGO GPI interferometer (resolution 1/8000), in which the PV and RMS values are 7.7210 μm and 1.9566 μm, respectively. The measurement results about the freeform surface in the experiment are summarized in Table 3.

According to Fig. 7 and Table 3, an obvious measurement error can be seen between the testing result with ZYGO interferometer and that with CMM-measured reverse Hartmann test system. In contrast, a good agreement, both in the shape and error magnitude, can be observed between ZYGO interferometer testing result and that from reverse Hartmann test after removing the geometrical error based on the proposed double-step calibration method. Thus, the proposed double-step calibration method provides a feasible way to calibrate the test system geometrical error and achieve accurate testing of complex freeform surface.

Optics EXPRESS

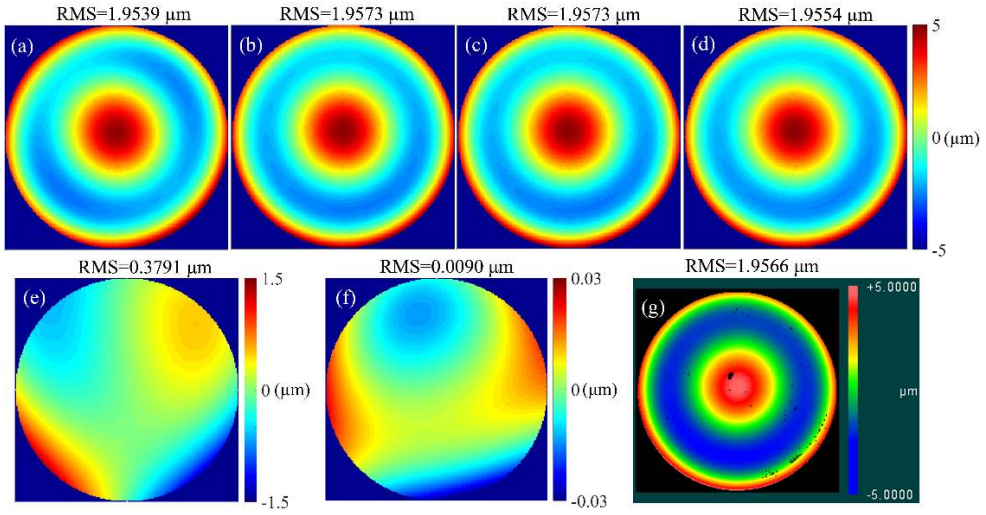

Fig. 7. Testing surface error in the experiment. Surface errors measured with reverse Hartmann test system (a) based on CMM-measured parameter, (b) after first-step calibration and (c) after second-step calibration, and the corresponding changes (e) after first-step calibration and (f) after second-step; (d) measured surface error after double-steps calibration with additional geometrical error; (g) surface error measured with ZYGO interferometer.

Table 3. PV and RMS values of testing surface error in the experiment

	PV (μm)	RMS (μm)
With system geometrical error	8.1915	1.9539
After first-step calibration	7.7377	1.9573
After second-step calibration	7.7301	1.9573
With additional geometrical error	7.7511	1.9554
ZYGO interferometer	7.7210	1.9566

4. Conclusion

A general accurate calibration method is present for the reflective surface testing based on reverse Hartmann test, in which the calibration of system geometry is required to achieve "null" testing. Based on the low-order Zernike aberration optimization and high-order aberration separation, the double-step calibration method is proposed to calibrate the system geometrical error with various weights in the geometric aberration. By separating the high-order geometric aberrations from various components in test system, the problem of over-correction can be solved effectively in calibration process, enabling the testing of freeform surface with high dynamic range. Both the computer simulation and experimental results confirm the accuracy and feasibility of the proposed geometrical error calibration technique, and a good measurement accuracy has been achieved. The proposed method provides a feasible way to achieve accurate testing of reflective surfaces with complex shapes, and lower the requirement on the calibration of test system geometry. Besides, the proposed general method also enables the calibration of large geometric errors in various testing system, such as the interferometers and deflectometric systems, etc.

Funding

Zhejiang Provincial Natural Science Foundation of China (LY17E050014); National Natural Science Foundation of China (NSFC) (51775528); Project of General Administration of Quality Supervision, Inspection & Quarantine of China (AQSIQ) (2017QK033); Guangxi Universities Key Lab of Optoelectronic Information Processing (KFJJ2017-02).